Biomaterials Advances 133 (2022) 112594

Contents lists available at ScienceDirect

Biomaterials Advances

journal homepage: www.elsevier.com/locate/bioadv

Development of zinc oxide/hydroxyapatite/poly(D,L-lactic acid) fibrous scaffold for tissue engineering applications

Victoria Padilla-Gainza [a,d], Heriberto Rodríguez-Tobías [a], Graciela Morales [a,*], Antonio Ledezma-Pérez [a], Carmen Alvarado-Canché [a], Raúl Loera-Valencia [a], Cristóbal Rodríguez [b], Robert Gilkerson [b], Carlos Trevino De Leo [c], Karen Lozano [d]

[a] Synthesis and Advanced Materials Departments, Centro de Investigación en Química Aplicada, Blvd. Enrique Reyna 140, Saltillo CP 25294, Coah, Mexico
[b] Biology Department, University of Texas Rio Grande Valley, 1201 West University Drive, Edinburg, TX 78539, USA
[c] Department of Physics and Astronomy, The University of Texas Rio Grande Valley, 1 W. University Blvd., Brownsville, TX 78500, USA
[d] Mechanical Engineering Department, University of Texas Rio Grande Valley, 1201 West University Drive, Edinburg, TX 78539, USA

ARTICLE INFO

Keywords:
Polymeric fibers
Biopolyesters
Forcespinning
Centrifugal spinning
Biocompatible scaffolds
Tissue engineering

ABSTRACT

Scaffolds based on polymeric fibers represent an engaging biomedical device due to their particular morphology and similarity with extracellular matrices. The biggest challenge to use fibrous materials in the biomedical field is related to their favorable platform for the adhesion of pathogenic microorganisms. Therefore, their optimum performance not only depends on their bioactive potential but also on their antimicrobial properties. The aim of this work was the design of antimicrobial (zinc oxide, ZnO) and bioactive (hydroxyapatite, Hap) fibrous materials using poly(D, L-lactic acid) (PDLLA) as the polymer fiber substrate. Fiber based composite scaffolds were developed using the Forcespinning® technique. For analysis purposes, the morphological, thermal, antimicrobial and biological properties of the fibrous hybrid system obtained at a concentration of 5 wt% of ZnO and 5 wt% of Hap were studied. The incorporation of the aforementioned nanoparticles (NPs) mixture in PDLLA led to an increase in viscosity and a pseudoplastic tendency of the precursor solution, which caused an increase in fiber diameters and their dispersion of values. Small cavities and certain roughness were the main surface morphology observed on the fibers before and after NPs incorporation. The fiber thermal stability decreased due to the presence of the NPs. The antimicrobial properties of the hybrid fibrous scaffold presented a growth inhibition (GI) of 70 and 85% for *E. coli* and *S. aureus* strains, respectively. Concerning the osteoblast-cell compatibility, PDLLA and hybrid PDLLA scaffold showed low toxicity (cell viabilities above 80%), allowing cell growth inside its three-dimension structure and favorable cell morphology extended along the fibers. This behavior suggests a promising potential of this hybrid PDLLA scaffold for bone application.

1. Introduction

Polymeric fibers have an important role in the development of biomedical materials. Fiber arrangement in a three-dimensional structure allows the design of architectures that promote cell adhesion and migration as well as transfer of vital substances for cell proliferation [1]. In the last decade, there has been a growing interest in the use of polymeric fiber scaffolds in the area of tissue engineering [2,3]. Polyester (polycaprolactone (PCL), poly (lactic acid) (PLA), poly (glycolic acid) (PLG) and poly (lactic-co-glycolic acid)) based scaffold systems have gained increasing attention given their biodegradability, biocompatibility and ease of processing [1].

For the design of polymeric fiber scaffolds, it is necessary to consider the incorporation of substances that would promote cell-scaffold interaction as the affected tissue regenerates. In the case of bone substitutes, hydroxyapatite (Hap) has been the most commonly used bioactive component, since it is the main inorganic constituent in the bone matrix [4,5]. Additionally, it has been shown that Hap contributes to important biological processes for bone regeneration, such as osteoconduction [6] (bone growth at the superficial level), osteoinduction [7] (pluripotent cells are stimulated to develop bone-forming cells, process that induces osteogenesis) and osseointegration [8] (stable anchoring of an implant, obtained by direct contact between bone tissue and implant) [8]. However, scaffold bioactivity can also increase by incorporating others ceramic biomaterials such as laponite nanosilicates, bioactive glasses, calcium phosphates, biphasic calcium phosphate, among others [9,10]. At present, different fibrous hybrid systems based on biopolyesters and Hap have been studied. In this context,

* Corresponding author.
E-mail addresses: victoria.padilla@utrgv.edu (V. Padilla-Gainza), graciela.morales@ciqa.edu.mx (G. Morales), Antonio.ledezma@ciqa.edu.mx (A. Ledezma-Pérez), carmen.alvarado@ciqa.edu.mx (C. Alvarado-Canché), raul.loera@ki.se (R. Loera-Valencia), robert.gilkerson@utrgv.edu (R. Gilkerson), karen.lozano@utrgv.edu (K. Lozano).

http://dx.doi.org/10.1016/j.msec.2021.112594
Received 4 August 2021; Received in revised form 2 November 2021; Accepted 2 December 2021
Available online 9 December 2021

it has been reported that these systems offer good support for the adhesion, growth and osteogenic differentiation of mesenchymal cells (hMSCs) [6,11,12], osteoblasts (MG-63) [13,14] and mouse pre-osteoblasts (MC3T3-E1) [15]; these results have been attributed mainly to the presence of Hap.

It is important to emphasize, the properties that promote cell adhesion and proliferation also favor the growth of bacteria [16]. Bacteria proliferation in this type of implants hampered its full adoption in tissue engineering applications [17–19]. Consequently, in the last decades, the incorporation of biocidal agents (antibiotics, organic substances, metals and metal oxides) as part of the implant components has been widely studied. There are different metals and metal oxide nanoparticles such as MgO, Ag, Fe_2O_3, TiO_2, CuO, Mg $(OH)_2$ and ZnO which have been used for biotechnological and biomedical applications. ZnO NPs (n-ZnO) have shown excellent antimicrobial activity and biocompatibility [20]. Additionally, ZnO combined with other materials (antibiotic or anti-inflammatory drugs, other metal oxide/metal doping, plant extracts, polymeric biomaterials/films and ZnO quantum dots) has showed a reinforced action against pathogenic microorganisms (*Escherichia coli*, *Staphylococcus aureus*, *Pseudomonas aeruginosa*, *Bacillus subtilis*, *Listeria monocytogenes*, etc.) and an enhance in its bioactive properties [21–23]. Previous studies have reported that n-ZnO has selective toxicity for bacteria but exhibits minimal detrimental effect on human cells [24]. In addition, it has been proven that it exerts an osteoconductive and osteoinductive effect in mesenchymal cells [25]. n-ZnO has a low production cost, effective control of its morphology, promotes surface interactions with different functional groups [26,27] and it appears on the *Generally Recognized List As Safe* (GRAS) from the American Food and Drug Administration (FDA). Therefore, making it an attractive antimicrobial agent for biomedical applications. Recently, green approaches for the synthesis of ZnO NPs have been proposed, such as biosynthesizing ZnO using *Lactobacillus* strain, *Aloe vera* peel extract, etc. [28,29]. Different studies of composite materials based on biopolyesters and ZnO have been reported [30–37]. In these reports, *E. coli* and *S. aureus*, appear to be the most widely studied strains with ZnO showing an antimicrobial effect on *S. aureus* strain with a grow inhibition (GI) above 95% at concentrations ≥1% of ZnO.

Regarding the hybrid systems with dual antibacterial and bioactive properties, just a few reports have been published using the ZnO/Hap combination. Zinc-doped Hap nanoparticles (nHap-Zn) have shown promising potential. Staníc et al. [38] reported antimicrobial activity of nHap-Zn in *E. coli* and *S. aureus* strains, showing a GI ≥ 97%. Gnaneshwar et al. [20] studied the biological effect of nHap-Zn as part of a system of electrospun polymeric fibers in human fetal osteoblast cells (hFOB), and evidenced an increased biological, enzymatic and biomineralization activity in systems made up with 2% of nHap-Zn. Ajinkya et al. [39] reported good antibacterial (*E. coli* and *S. aureus*), bioactive (human osteosarcoma cell, MG-63) and mechanical performance of electrospun materials based on PCL/Hap/ZnO at ZnO concentration ≤ 10%.

The strategic combination of bioactive (Hap) and antimicrobial (ZnO) properties in a biodegradable and biocompatible polymer matrix is attractive to produce hybrid materials targeted for applications related to tissue engineering. Therefore, in this work the production of antibacterial/bioactive fibrous scaffolds with the potential to be used in the regeneration of bone tissue is studied using a high production and low-cost fiber-based system production technique. Forcespinning® [40–42] is a centrifugal spinning technique not widely explored in this field, which opens the possibility of establishing an understanding of the characteristics of hybrid materials obtained under the influence of specific parameters and conditions with proven industrial scale-up.

Based on the authors' knowledge, no reports have been published using PLA as polymeric matrix with the proposed nanoparticle combination. This work reports the operating conditions to obtain hybrid materials based on homogeneous poly(D,L-lactic acid) fibers (PDLLA) with n-ZnO and n-Hap through the centrifugal spinning technique, Forcespinning®. In addition, an analysis of the influence of NPs on the rheology of the precursor solutions, morphological characteristics, thermal and mechanical performance, antibacterial and biological activity of the obtained hybrid materials is established.

2. Experimental methodology

2.1. Materials and reagent

PDLLA provided by NatureWorks LLC (Ingeo 6362D) with Mw = 160 kg·mol^{-1} and Đ = 1.646 was used as the polymer matrix. The solvent used for the polymer solution was chloroform, ACS grade, provided by Fisher Scientific. n-ZnO NPs were synthesized under a procedure described in a previous work [43]. Hydroxyapatite (Hap), Dp ≤ 200 nm and 97% of purity, was obtained from Sigma-Aldrich.

2.2. Preparation of the precursor solutions

To obtain PDLLA fibers with 5 wt% of n-Hap and 5 wt% of n-ZnO, 20 g of precursor solutions containing PLA, n-Hap, n-ZnO and chloroform ($CHCl_3$) in the amounts of 0.200, 0.011, 0.011, and 19.800 g respectively were prepared. Dispersions of n-ZnO and n-Hap in $CHCl_3$ were prepared by using an ultrasound bath (Cole-Parmer 8891) for 50 min. Once the dispersion process was completed, PDLLA was added to the system to obtain the corresponding solution at 10 wt%. The solutions were agitated in a stir plate (Thermo Scientific, Cimarec+ series) between 400 and 600 rpm for 22 h at room temperature. The viscosities of the solutions were determined using an Anton Paar rheometer, Physica model MCR 302 with a cone-plate configuration (diameter 50 mm, angle of 2 and gap of 0.205) at 25 °C.

2.3. Centrifugal spinning process

The prepared precursor solutions were subjected to a centrifugal spinning process in a Cyclone L-1000 M (FiberRio Technology, Corp.), which consists of a cylindrical spinneret with two nozzles equipped with regular beveled needles (30-gauge length, Becton, Dickinson and Company) and eight collectors in the form of metal bars arranged around the spinneret at a distance of 15 cm from the nozzles. For each run, 2 mL of polymer solution were added to the spinneret, and fiber spinning was carried out for 5 min at a temperature of 23 ± 3 °C with a relative humidity of 59.3% ± 9.6%. It is important to mention that the fiber characterization in the optimization stage was determined from the fibers collected from a single run (5 min). Once proper parameters were established, the resultant mats were obtained by the collection of 7 runs (5 min each). The fibers were placed in a vacuum oven at 30 °C for 24 h, to remove any residual solvent. Finally, the fibers were stored in plastic bags in the presence of a desiccant for moisture control.

2.4. Experimental design

The polymer concentrations of the precursor solutions were established based on a previously published optimization study (10 wt% of PDLLA) [44]. Similarly, considering the antimicrobial evaluation previously reported by the research team [43], the concentration of ZnO was selected based on the minimum concentration necessary to achieve inhibition of bacterial growth above 97%; which was 5 wt%. Regarding the Hap concentration, through a cell viability study [45], a value of 5 wt% was selected. The adjustment of the angular speed (ω) (7000–10,000 rpm) was made considering the influence that the incorporation of the mixture of ZnO-Hap had on the rheological behavior of the precursor solutions.

For the selection of the optimum ω, fiber morphology, fiber diameter, and ultimate yield were considered. The yield/output of the process (ηp) was estimated by Eq. (1).

$$\eta_P = \frac{M_{mf}}{ST} \times 100 \quad (1)$$

where M_{mf} and ST are the grams of fibers collected per run (5 min) and the total solids (polymer + NPs) contained in 2 mL of polymer solution, respectively.

2.5. Fibrous material characterization

The morphological analysis was carried out using a scanning electron microscope (Carl Zeiss, Sigma VP). The images obtained were analyzed with the Image J software (v. 1.48) to estimate average fiber diameters (D_f) and average pore size (interfibrillar spaces). Diameter distributions were obtained by measuring 100 fibers (20 fibers per micrograph) with three measurements per fiber, making a total of 300 measurements per sample. Obtained data was represented by means of box-bars charts, where the boxes reflect 50% of the population of values located between quartile 1 (Q_1 = 25% of the population) and 3 (Q_3 = 75% of the population) and the bars represent the amplitude of the distribution according to the most probable values or those that appear more frequently. The distribution and dispersion of the n-Hap and ZnO within the fibers were determined using energy dispersive X-ray spectroscopy (EDS, EDAX Octane Super).

For the calculation of the scaffold's porosity, an adjustment of the equation reported by Wang et al. [46] was used (Eq. (2)),

$$\varnothing = \left(1 - \frac{m}{Z*A*H*\rho}\right)*100 \quad (2)$$

where m, Z, A, H, and ρ are the mass, thickness, width, and length of the scaffold and the density of the polymer with n-Hap in the corresponding case, respectively.

The surface roughness was determined through atomic force microscopy (AFM) (NT-MDT spectrum instrument, SOLVER Nano) operating in semi-contact mode with a NSG01 series single crystal silicon tip, N-type, 0.01–0.025 Ohm-cm, antimony doped. The roughness (Ra) was determined using the average of three to five measurements of the most representative surfaces on the top of the fiber over 5 μm^2 areas using muscovite mica sheet as a substrate.

Thermal properties were evaluated through thermogravimetric analysis (TGA) (TA Instruments, Q400) and differential scanning calorimetry (DSC) (TA Instruments, Q200). To perform the TGA, the samples were heated from 30 to 600 °C under a nitrogen atmosphere, at a heating rate of 10 °C min^{-1}. Regarding the DSC, the heating was carried out from 70 to 200 °C at a rate of 10 °C min^{-1}, the samples were isothermally maintained at 200 °C for 2 min and then cooled down at the same rate to −70 °C. A second heating cycle under the same conditions was conducted.

Mechanical properties of the fibrous materials were determined by tensile tests using the universal testing machine (Tinius-Olsen, H10KS). The tensile testing was made using the paper frame method [47,48]. To this end, test pieces of 32 mm long and 3 mm wide were cut and conditioned for 24 h at room temperature (23–25 °C). The tensile tests were carried out at a deformation speed of 2 mm.min^{-1} with a clamp separation of 27.5 mm, using a 50 N load cell (five repetitions).

2.6. Antibacterial properties

The evaluation of the antibacterial activity of the fibrous materials was made taking as reference the Japanese Industrial Standard, Z280126 [49]. The test was performed for two microorganisms of clinical importance, *Escherichia coli* ATCC-25922 and *Staphylococcus aureus* ATCC-29213. For the test, 2 × 2 cm samples under aseptic conditions were inoculated with 4 mL of a microorganism suspension in trypticase soy broth, equivalent to 50,000 colony forming units per mL (CFU $m{\cdot}L^{-1}$). Subsequently, the samples were incubated at a temperature of 37 °C and 90% humidity for 24 h. At the end of the incubation time the population of microorganisms present in the samples was determined (the tests were done in quadruplicate), and the antibacterial activity (R) was calculated using Eq. (3):

$$R = \left(\log \frac{B_t}{B_0} - \log \frac{M_t}{B_0}\right) \quad (3)$$

where B_0 and B_t are the amounts in CFU$\cdot mL^{-1}$ of bacteria that survive in the presence of the reference (material without n-ZnO) before and after 24 h of incubation, respectively. M_t is the amount of bacteria that survive after 24 h of incubation in the presence of the antimicrobial material (material with n-ZnO). Additionally, the inhibition to bacterial growth (GI) was determined by means of Eq. (4):

$$GI = \left(\frac{B_t - M_t}{B_t}\right) \times 100 \quad (4)$$

2.7. Biological test

2.7.1. Cell viability

A mouse pre-osteoblast cell line (MC3T3-E1) was used to test the ability of fibers to support cell growth. The cells were cultured in MEM Alpha medium (1×) supplemented with 10% fetal bovine serum (FBS), 100 international units per milliliter (IU$\cdot mL^{-1}$) of penicillin and 100 μg$\cdot mL^{-1}$ of streptomycin. 30,000 cells were inoculated into 1 × 1 cm samples of fibrous material, previously sterilized with UV light for 10 min, and incubated at 37 °C (5% CO_2 in a controlled atmosphere) in 48-well culture plates. After incubation for periods of 1, 3, 5 and 7 days, the culture medium was removed and 300 μL of resazurin solution (combined in a fresh culture medium ratio of 1:10) were added, allowing the resazurin to react for 4 h. Immediately afterward, a volume of 150 μL was taken from each sample to determine the fluorescence on a microplate absorbance reader (iMark™ Bio-Rad) at a wavelength of 570 nm.

2.7.2. Cell morphology and proliferation

Confocal microscopy was employed to evaluate cell morphology at day 7. After incubation, samples seeded with MC3T3 cells were lifted and placed in a new dish to removed non-adherent cells. Cells were stained with Mito Tracker Red (Invitrogen) to identify mitochondrial morphology, washed with culture medium twice, and then with phosphate buffered saline (1xPBS). Cells were then fixed with 2 mL of a 4% formaldehyde solution in PBS. Finally, they were stained with 4′, 6-diamidino-2-phenylindole (DAPI) to label cell nuclei, washed, then mounted with 50% glycerol and prepared for their respective microscopic analysis. Confocal laser scanning fluorescence microscopy (Olympus FV10i microscope) was used for the cell visualization.

To visualize the full extent of cellular morphology, samples were labeled with the actin-binding dye phalloidin AlexaFluor™ 488 (Invitrogen). As above, cells were fixed with 4% formaldehyde and washed twice with 1xPBS. Samples were then labeled with 100 μL of a DAPI-Phalloidin

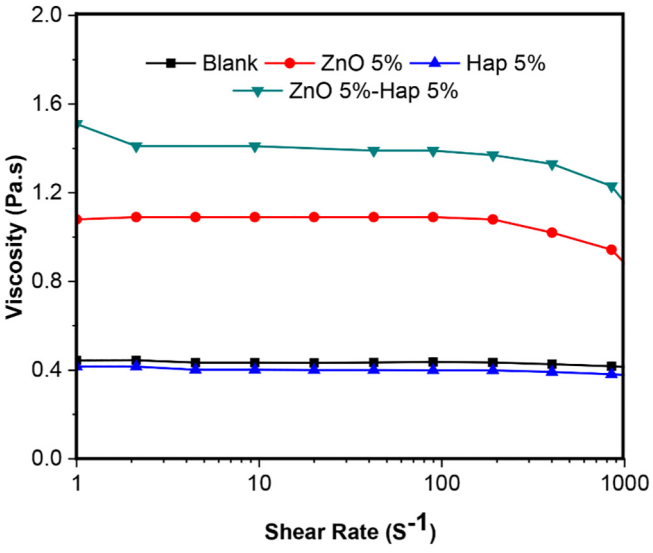

Fig. 1. Rheological behavior of PDLLA precursor solutions containing ZnO 5%-Hap 5%, n-ZnO 5%, n-Hap 5% and without NPs (blank).

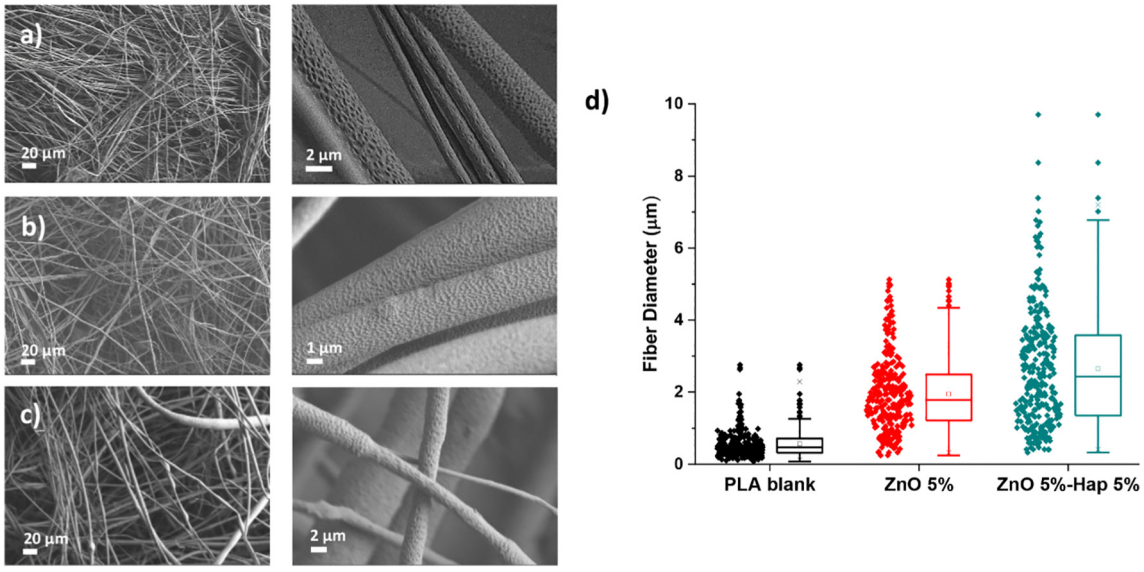

Fig. 2. SEM images of the PDLLA blank (a), ZnO 5% (b), ZnO 5%-Hap 5% (c), and the box chart of fiber diameters for each system (d), obtained at 9000 rpm.

mixture (ratio: 2 µL-Phalloidin/1 µL-DAPI/1000 µL-PBS) for 10 min at room temperature in the dark. After treatment, the samples were washed twice with 1 × PBS and mounted with 50% glycerol for confocal microscopy (Olympus FV10i microscope).

To assess cell proliferation, a quantitative analysis was performed. The number of cells found in ten randomly selected images (area size: 212 × 212 µm) were considered for the study. The number of independent experiments (biological replicates) was 3. These cells were counted and averaged. Results were represented through the mean +/− standard error, as the average number of cells per image.

2.7.3. Depths profile study

Three-dimensional segmentation. Confocal images were segmented using the 3D image processing software Imaris 9.1 (Bitplane AG, Zurich, Switzerland). Z-stacks were processed using the volume tool to segment the phalloidin and DAPI signals to reconstruct volumes for the cytoskeleton

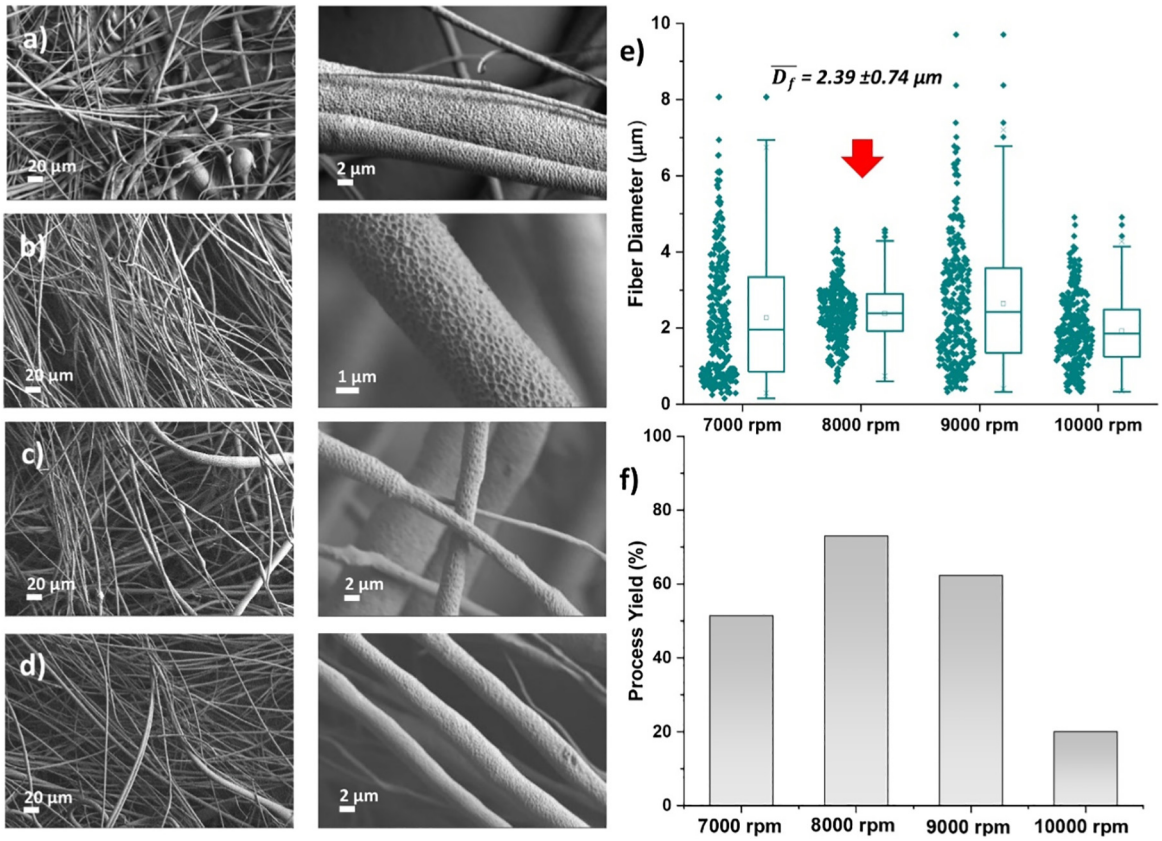

Fig. 3. SEM images of PDLLA-ZnO 5%-Hap 5% systems obtained at different ω, 7000 rpm (a), 8000 rpm (b), 9000 rpm (c), 10,000 rpm (d), box plot of fiber diameters for each system (e), and process yields (ηp) (f).

and nucleus, whereas the phase contrast signal was processed using the dots module to represent the spatial distribution of the material in relationship to cells. Background subtraction was carried out for all channels. Metadata of the 3D-reconstructions can be shared upon request and are available in the original high-resolution .TIFF files.

3. Results and discussion

3.1. Rheological study of polymeric solutions

The apparent viscosities of the precursor polymer solutions of PDLLA with their corresponding nanoparticle concentration were evaluated as a function of shear rate. Fig. 1 shows the results obtained from the developed composite systems and their respective reference systems used for comparison: blank and binary systems formulated with each NPs. The presence of NPS in PDLLA-ZnO 5% and PDLLA-ZnO 5%-Hap 5% systems produced an increase in viscosity and show a pseudoplastic tendency, behavior that denotes significant interactions among the components. On the contrary, PDLLA-Hap 5% shows a decrease in the viscosity in comparison with the pristine system.

Regarding the systems with ZnO, it has been described that the hydrogen bridge-type interactions between the polymer and the n-ZnO, can cause an increase in the viscosity of the precursor solutions as the concentration of NPs increases [50,51]. Regarding the Hap, the decrease in the viscosity was also attributed to strong polymer-NPs interactions [52,53]. In this case, the Hap size (44.4 ± 36.3 nm) (Supplementary Material, Fig. S1), which is approximately 6 times greater than that of ZnO (6.36 ± 2.08 nm), had an effect on the viscosity as well. Taking into consideration that the Hap size is in the order of the radius of gyration of the polymer (30–40 nm) [54], the Hap particles could act as a mean for polymer adsorption; leading to a lower proportion of free polymer chains capable of interacting with the solvent [55]. This phenomenon could explain the observed decrease in the viscosity [45]. With respect to the incorporation of the ZnO-Hap mixture into the PDLLA system, there was a slight increase

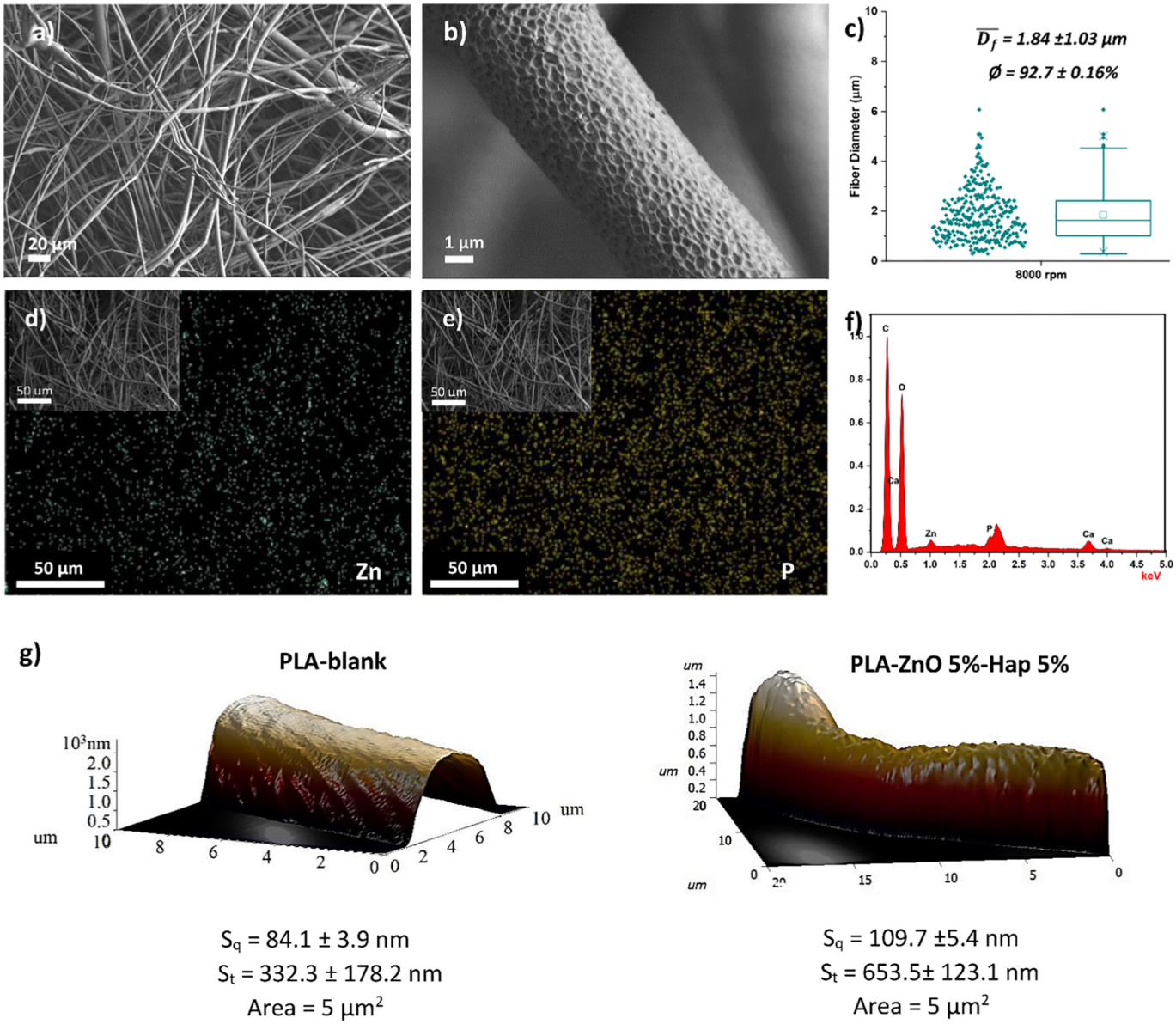

Fig. 4. SEM images (a, b), box charts of fiber diameters (c), elemental mapping of zinc (d) and phosphorus (e), and EDS spectrum (f) of the PDLLA-ZnO 5%-Hap 5% obtained using the condition selected in the optimization phase. (g) AFM topography of a fiber surface profile and corresponding roughness parameters, root-mean-square roughness (S_q) and peak to valley height roughness (S_t).

in the viscosity of the solution compared to that obtained with 5% n-ZnO alone. This could be attributed to a synergetic effect of the combined NPs on the viscosity.

The FTIR spectrum of the polymer solutions (Supplementary Material, Fig. S2) shows a displacement of the carbonyl group band towards a higher vibration frequency in the PDLLA solution (PDLLA-$CHCl_3$, without NPs), mainly produced by the inductive effect generated due to the solvent-polymer interaction. On the other hand, the incorporation of n-ZnO did not generate a change in the displacement of the carbonyl group, but a wider band was observed, which could indicate a greater number of interactions. Spectra from the Hap and mixture of NPs (ZnO-Hap) presents bands with a similar behavior, a lower displacement of the carbonyl group band compared to the polymeric solution without NPs.

3.2. Effect of NPs and angular speed on fiber formation.

Fig. 2 shows the SEM micrographs of the pristine PDLLA (Fig. 2a) and PDLLA-NPs fibers (Fig. 2a–c), and the corresponding box and bar diagrams for D_f dispersions. Fibers of the ternary system (Fig. 2c) have a surface roughness slightly higher than that observed in the absence of NPs (see Section 3.3.1). Based on these results, it could be stated that the surface appearance is mainly determined by the nature of the polymer-solvent system. Regarding the uniformity of the fibers, some thin sections are evidenced, possibly due to the heterogeneous distribution of the NPs throughout the fibers, as well as to the pseudo-plastic characteristics of the precursor polymer dispersion. In the uniaxial stretching process of a polymeric fluid, the molecules are forced to align themselves in the direction of the applied stress; however, when the fluid is highly elastic, the aligned chains tend to relax to assume their original non-aligned conformation, a behavior that could counteract the formation of homogeneous fibers [56].

Concerning the dispersion of D_f (Fig. 2d) there is a relationship between rheological behavior and fiber size. As the viscosity and the pseudo-plastic tendency of the precursor solution increases, at a constant angular speed, in this case, 9000 rpm, there is a displacement of the diameter dispersion towards higher values with a wider distribution. For the pristine, binary and ternary systems, 50% of the population of diameters between Q_1 and Q_3 were found in the intervals from 0.32 to 0.72 μm, 1.21 to 2.48 μm and 1.34 to 3.58 μm, respectively.

Table 1
Residues obtained at 600 °C through TGA of the PDLLA systems at different concentrations of ZnO, Hap and ZnO-Hap.

Systems	R_{est} (%)	R_{real} (%)
Blank	0.21	0.21
ZnO 5%	4.95	4.05
Hap 5%	5.15	5.39
ZnO 5%-Hap 5%	9.89	7.80

Due to the rheological changes presented by the precursor solution with the incorporation of the ZnO-Hap mixture, different angular speeds (7000–10,000 rpm) were evaluated in order to determine the best fiber production conditions (Fig. 3). At 8000 rpm, the formation of more homogeneous fibers was observed, with a higher production yield (>70%) and narrower fiber diameter distribution. Therefore, 8000 rpm was selected for subsequent fibrous scaffold production.

3.3. Morphological, thermal, and mechanical characterization

3.3.1. Morphology

Based on the optimization phase described in the previous section, the scaffolds were manufactured at ω of 8000 rpm; resulting in mostly homogeneous, long, continuous fibers with some small defects (Fig. 4a). As described, the fibers have a rough surface morphology (Fig. 4b). Specifically, the NPs incorporation produced a slight increase in the surface roughness, obtaining a root-mean-square roughness (S_q) of 84.1 and 109.7 nm for PDLLA blank and PDLLA-ZnO 5%-Hap 5%, respectively (Fig. 4g). These differences should not represent a high impact on cell adhesion given that the roughness is in the nanometer scale [57]. Regarding the dispersion of fiber diameters, this was presented in a slightly wider range than that obtained in the optimization phase (Fig. 4c).

The porosity Ø, defined in a 3-D fiber scaffold structure as the space between fibers; was determined through Eq. (2) (Fig. 4c) to be greater than 90%. Additionally, through the Image J software, the area distribution between fibers was determined. It was found that 50% of the population has an area above 30 μm^2 and the values are distributed from 2 to 2561.7 μm^2. These results show that part of the pore distribution has sizes large enough to guarantee cell migration (Supplementary Material, Fig. S3) [5,58].

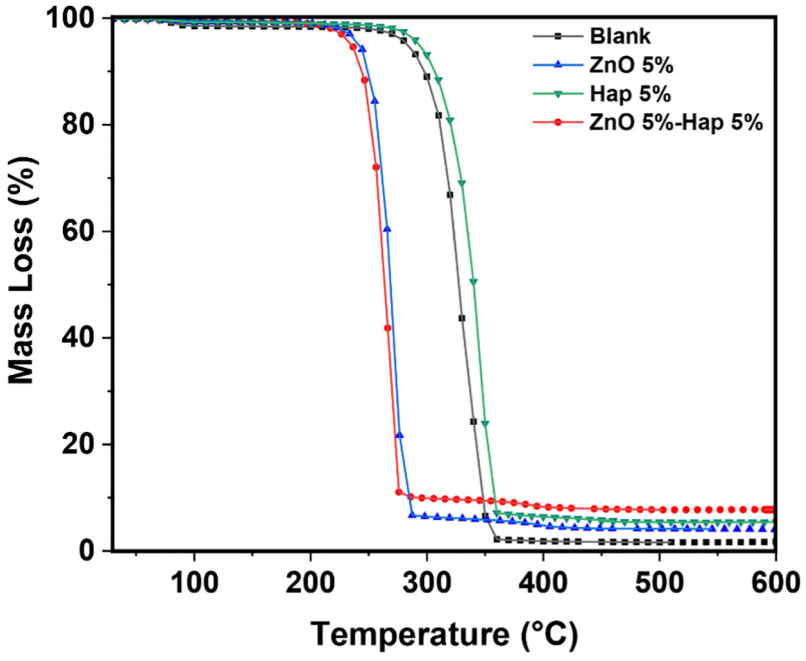

Fig. 5. TGA thermograms of PDLLA fibers, obtained with ZnO, Hap and ZnO-Hap.

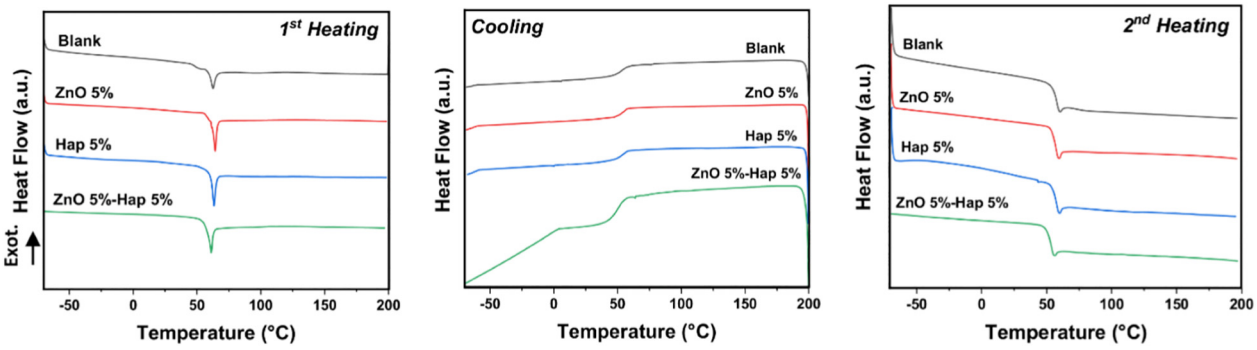

Fig. 6. DSC thermograms of PDLLA fibers with ZnO, Hap and ZnO-Hap.

Through EDS spectrum and elemental mapping, the presence of NPs in the fibers was evidenced (Fig. 4d–f). In all the analyzed areas, both NPs were identified, observing more agglomeration points for n-ZnO. It must be pointed out that n-ZnO size (6.36 ± 2.08 nm) is six times smaller than that of Hap (44.4 ± 36.3 nm), reason why there is a strong tendency of n-ZnO to form agglomerates in order to diminish their high surface energy.

3.3.2. Thermal properties

In Fig. 5, the thermo-degradation patterns of the materials formulated without (blank) and with NPs are presented. In the first instance, it was evidenced for ternary and binary systems, that the residue differs from the initial concentration. In Table 1, the estimated residue (R_{est}) and the real one (R_{real}) obtained at 600 °C are presented. Specifically, in the ternary system, the results were 9.89 and 7.80% for R_{est} and R_{real}, respectively. This difference is associated with the heterogeneous distribution of the NPs in the polymeric matrix, more specifically to the n-ZnO, due to the level of agglomeration reflected in the elemental mapping (Fig. 4d). Likewise, the loss of n-NPs, during fiber production should also be considered.

Regarding the thermal stability of the materials, degradation temperatures of 290, 242, 293 and 235 °C were presented for the blank, ZnO 5%, Hap 5% and ZnO 5%-Hap 5%, respectively. In the case of the ternary system, a decrease in thermal stability is observed, comparable to that presented by the system obtained at 5% ZnO. Despite the fact that Hap slightly increases the thermal stability of the fibers, the n-ZnO in the ternary system had a dominant effect, producing a degradation equivalent to the system formulated with 5% ZnO. Different publications attribute this behavior to the fact that ZnO promotes transesterification and depolymerization reactions of PLA [59–61].

Regarding the thermal transitions experienced by the materials, Fig. 6 shows the DSC thermograms of the heating-cooling-heating cycle. In these systems, it is typical to observe on the first heating an endothermic transition that occurs followed by the glass transition of the polymer [43]. In the ternary system, this transition occurs at slightly lower temperature (61.09 °C) when compared to the rest of the systems. On the other hand, during the cooling and second heating cycle, only a second order transition (T_g), typical of an amorphous polymer is shown and at lower temperature due to the incorporation of the mixture of NPs (ZnO 5%-Hap 5%) (Supplementary Material, Table S1).

3.3.3. Mechanical properties

Fig. 7 shows the mechanical performance of ternary materials and their corresponding binary systems, for comparative purposes. The PDLLA-ZnO 5%-Hap 5% system presented a marked decrease in its mechanical properties compared to the reference systems. As described in the previous sections, a concentration of around 5% of n-ZnO favors the formation of aggregates that lead to a reduction in the mechanical performance. These aggregates act as stress concentrators promoting the failure of the material. The incorporation of Hap, even though its distribution was more homogeneous, also had a negative effect on mechanical properties, for the same reasons described for n-ZnO. These results corroborate the important role of NPs size and their distribution in the mechanical performance.

3.4. Antibacterial properties

Fig. 8 shows the antibacterial efficiency of the materials evaluated with *E. coli* and *S. aureus*. As it can be seen, the incorporation of n-Hap produced

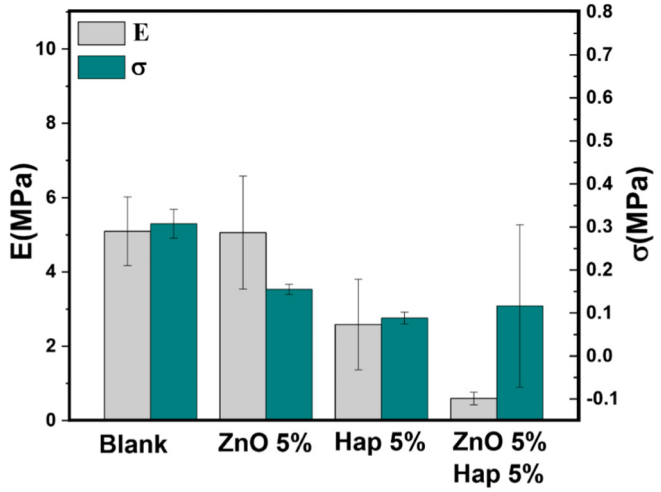

Fig. 7. Young's modulus (E) and tensile strength (σ) of the materials obtained with PDLLA, ZnO, Hap, and ZnO-Hap.

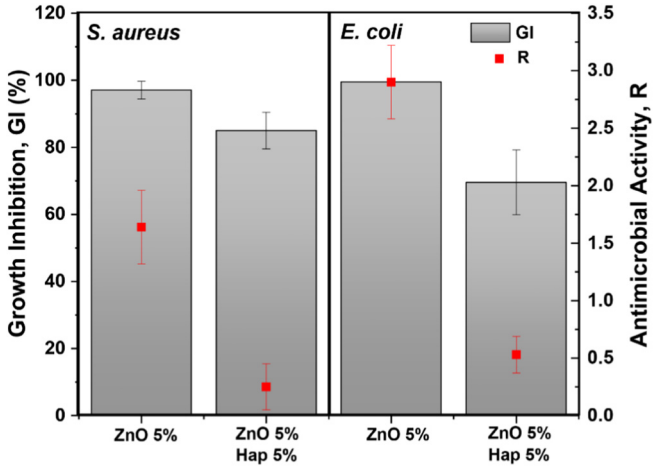

Fig. 8. Antimicrobial activity (R) and *S. aureus/E. coli* Growth inhibition (GI) of the PDLLA fibrous materials obtained with ZnO and ZnO-Hap.

a decrease in growth inhibition (GI) approx. 30 and 12% for *E. coli* and *S. aureus*, respectively, compared to the system formulated with 5% ZnO.

Saha et al. [62] obtained a similar behavior in the antimicrobial evaluation of a Hap-ZnO biocomposites. In their study the authors argued that Hap and ZnO distribution interfered with the antimicrobial performance of the biocomposite, without obtaining a total inhibition of the evaluated bacteria (*E. coli* and *S. aureus*) in 4 h of incubation. On the other hand, Felice et al. [63] reported a 99% inhibition of *S. aureus* strains with an electrospun fiber material based on poly(ε-caprolactone) (PCL), Hap and 1% of ZnO, after 18 h incubation.

However, the surface electrical charge of the materials is another important aspect that affects the behavior of bacteria and has to be considered in their antibacterial performance. As it has already been reported in different studies, the electrical charges of bacteria are negative, being the *E. coli* charge greater than that of *S. aureus* [64,65]. Regarding the surface charge of the fibers, the negative partial charge due to the ester group, could have influenced the adhesion process of the bacteria, causing inhibition in their growth. On the other hand, Hap has an isoelectric point (PI) of 7, presenting a positive charge at acidic pH [66]. In this sense, Hap could provide an attractive surface for bacteria promoting the adhesion and growth of bacteria. In this regard, Villareal-Gomez et al. [67] reported that the bacterial adhesion properties observed in PDLLA-Hap scaffolds are possibly due to the presence of polar groups in the Hap. Consequently, it could be argued that n-Hap exerted a shielding effect, affecting the antimicrobial performance of the ternary materials.

Regarding ZnO, it has a PI between 9 and 10. Yu et al. [68] determined that n-ZnO in distilled water (pH approx. 5) has a Z potential of 17 mV. In the case that the surface electrical charge would favor the adhesion of the bacteria, it must be considered that unlike Hap, ZnO does have a toxic effect on bacteria. Therefore, a positive surface charge would favor the antimicrobial action of ZnO into de fibrous material. Additional to the above aforementioned, other factors that could affect the antibacterial performance of the scaffolds are: 1) dispersion of NPs; as it could be observed in Fig. 4d, ZnO NPs showed a certain degree of aggregation, which produces a decrease in their surface area and therefore, in active points of interaction; 2) real concentration of ZnO; in the thermogravimetric analysis, the concentration of NPs mixture was lower than expected, thus a lower ZnO concentration will produce less antimicrobial action; and finally 3) the embedded NPs fraction will not have a direct interaction with the bacteria during 24 h of analysis.

The most frequently reported mechanisms of ZnO antimicrobial action have been: 1) rupture of the cell membrane by contact with n-ZnO; 2) release of Zn^{2+} ions; and 3) generation of reactive oxygen species (ROS), as a result of photocatalytic activity (activation by UV or visible light). This last mechanism is ruled out in this study, since the samples were incubated without UV irradiation, which is essential for the formation of ROS. On the other hand, in a study carried out by Felice et al. [63] the antimicrobial action was evaluated in polymeric fibers with different degrees of degradation, identifying the release of Zn^{2+} ions as the main mechanism of antimicrobial action. Based on the foregoing, it is considered, due to the characteristics of the systems designed in this work, that both direct contact with n-ZnO and the release of Zn^{2+} ions could be the responsible mechanisms for the observed antimicrobial action.

3.5. Biological properties

3.5.1. Cell viability

Cell viability assesses the cell mitochondrial metabolic activity, which is a semi-autonomous region of cells that is responsible for producing all the energy that the cells require to carry out their functions. In Fig. 9-a, the

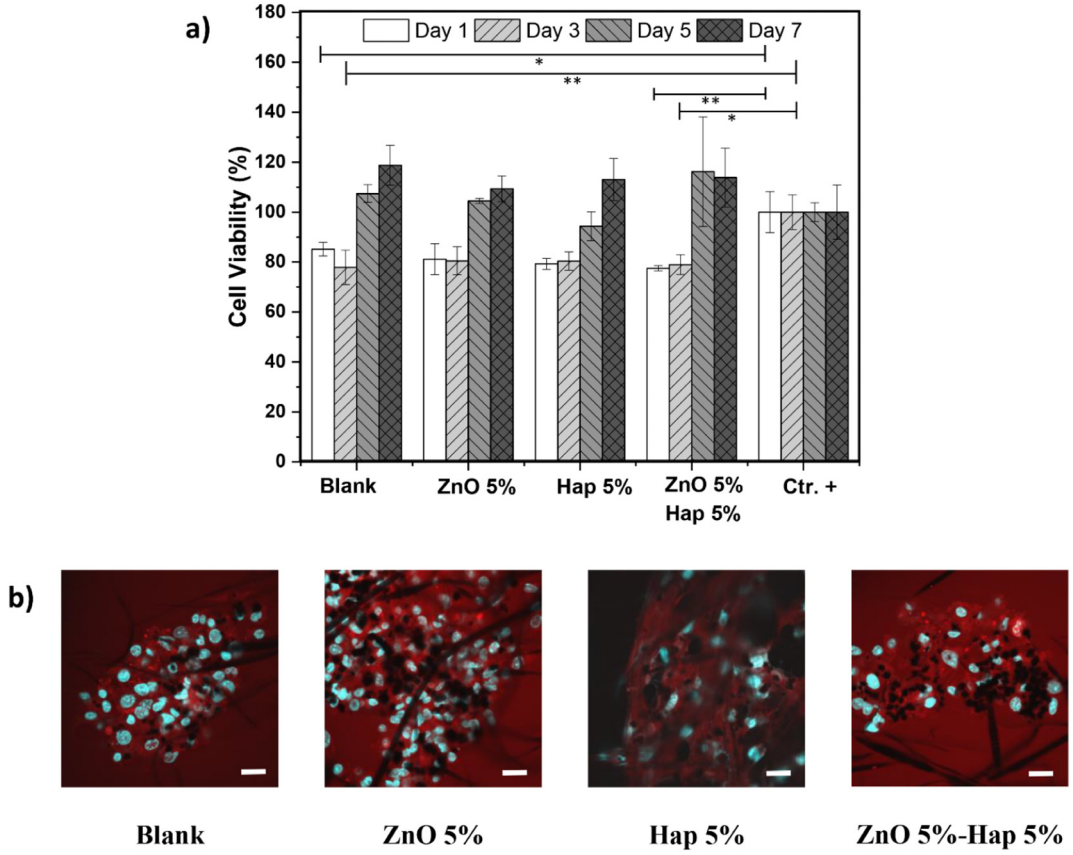

Fig. 9. a) Resazurin-MC3T3-E1 Cells Viability Test; Ctr. +: positive control (cells grown on glass coverslips) was taken as reference to determine the cell viability of the systems. Blank is defined by cell interacting with a PDLLA fiber without NPs. The results are presented as the mean of three experiments ± the standard deviation of the mean (*$p < 0.05$, **$p < 0.01$). b) MC3T3-E1 Confocal micrographs obtained at day 7 of scaffold-cell interaction, after being subject to the cell viability test (scale bar: 20 μm).

cell viability of the designed scaffolds is observed in relation to the positive control (Crt. +), defined by cells interacting with glass coverslips and blank defined by cell interacting with a PDLLA fiber without NPs. PDLLA fibers, either alone or incorporating ZnO and/or Hap, show an increased cell viability (above 80%) over the time course of days 1, 3, 5, 7, consistent with increased cell number as the MC3T3-E1 proliferate within the nanofiber scaffold environment.

The fact that the PDLLA scaffolds have shown viabilities above 100% with respect to the positive control, suggested that the positive control cells were near confluency; therefore, no significant changes in metabolic activity were evidenced for those last days. On the contrary, the scaffolds, due to a greater surface area and adequate pore size, allowed cells to continue proliferating. However, since the results for days 5 and 7 did not present statistically significant variations, complementary studies were required to elucidate the scaffold influence on cell behavior. For this reason, the study of cell morphology and proliferation is further addressed.

Fig. 9-b shows confocal micrographs of cells grown on fibers for the cell viability test (7 days). Mitochondria are labeled with Mitotracker (red), while DAPI labels cell nuclei (blue). An important feature is the presence of cell clusters/agglomerates in all systems. After 7 days, all scaffolds examined promoted the growth of MC3T3-E1 cells in clusters within the nanofiber matrix. Furthermore, the mitochondria morphology shows an interconnected network, representing an efficient system to deliver energy or transfer calcium between different areas of the cell [69,70].

3.5.2. Scaffold-cell interaction and proliferation

The ability of the examined scaffolds to support cell proliferation and adhesion test is depicted in Figs. 10–12. As the major determinant of cell shape, dynamics, and movement [71], the actin cytoskeleton was monitored to examine cell presence within scaffold matrix. In Fig. 10-a, the morphology of osteoblast cells contained in a PDLLA scaffold is visualized by labeling actin cytoskeletal filaments (Phalloidin) and nucleus (DAPI). It is clearly observed that the cells lay on the fibers and surround them, while extending in the direction of the fiber, (Fig. 10-a, Merge). Studies carried out by several authors with the same cell line, found that indeed an extended morphology favors cell performance [72,73]. The PDLLA blank and PDLLA-ZnO 5%-Hap 5% (Fig. 10-b), evidenced the formation of cell agglomerates, similar to those observed in Fig. 9-b. Both systems showed

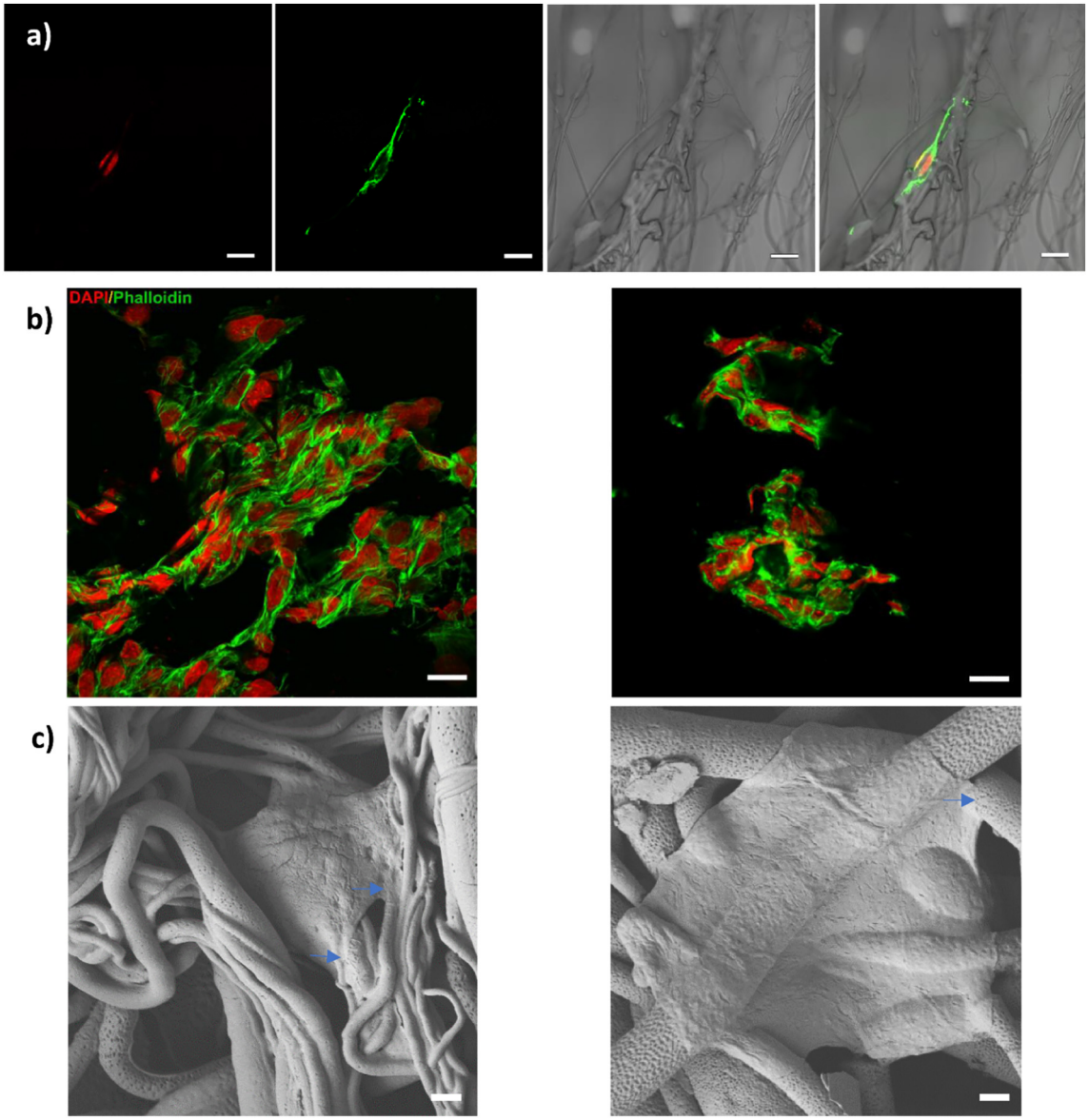

Fig. 10. Osteoblast cells (MC3T3-E1) morphologies observed in PDLLA fiber scaffolds obtained through confocal microscopy: a) cell and fiber interaction representation, b) Cell clusters found in day 5 (PDLLA blank) and 7 (PDLLA-ZnO 5%-Hap 5%) of the scaffold-cell interaction test (scale bar: 20 μm), and c) SEM images of the osteoblast cells interacting with the fibers from PDLLA blank and PDLLA-ZnO 5%-Hap 5%, left and right side, respectively (day 7) (scale bar: 2 μm).

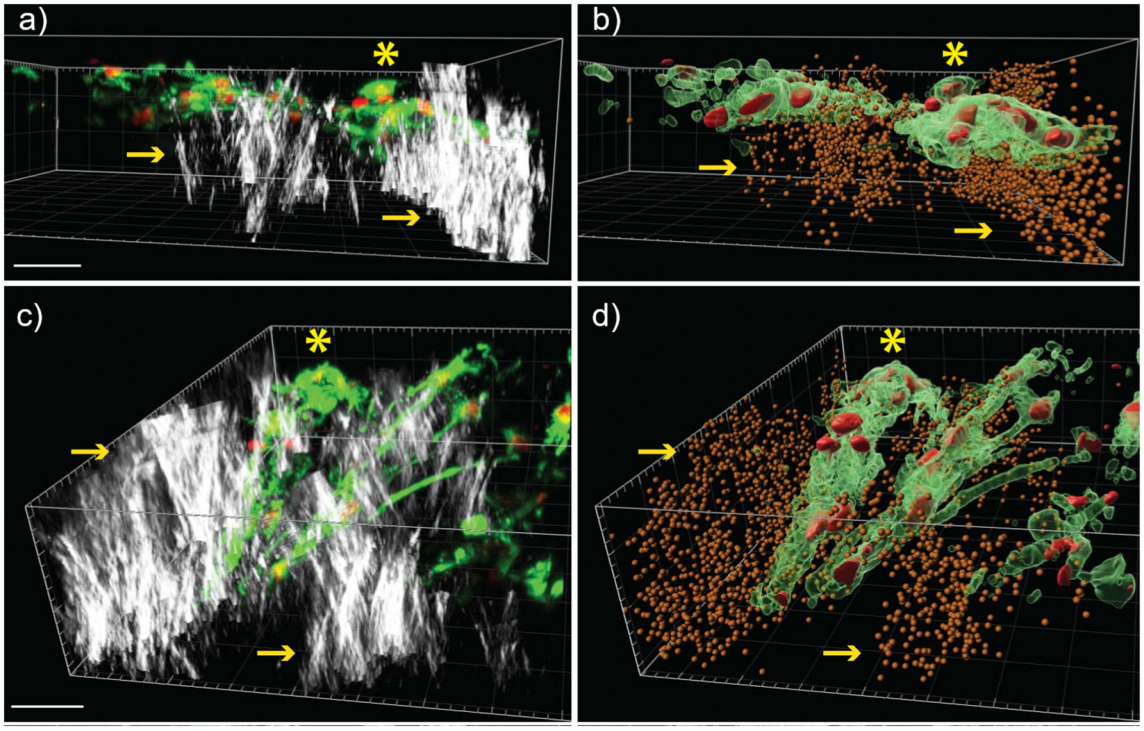

Fig. 11. MC3T3-E1 cells grow embedded in PDLLA-ZnO 5%-Hap 5% fiber scaffolds in three-dimensions. Lateral and upper view of fluorescence confocal Z-stacks (a and c, respectively) showing the cell cytoplasm (green) and nucleus (red) of MC3T3-E1 cells (yellow asterisks) into the PDLLA-ZnO 5%-Hap 5% fiber scaffolds (white), pointed by yellow arrows, for day 7 of cell-scaffold interaction. Imaris three-dimensional reconstruction of the fluorescent signal for cytoplasm, nucleus, and fiber scaffolds (represented as orange dots for better viewing) are shown in b) and d). Scale bar for all figures is 30 μm.

normal cell morphology and no signs of necrosis/apoptosis was found in the preparations; however, the cells in the blank showed a widely spread morphology, while the PDLLA-ZnO 5%-Hap 5% produced a more spindle-like morphology, probably due to the nature of its interaction with the cells. In Fig. 10-c, the SEM imaging reveals osteoblast cells spread on top of some fibers for the blank and ternary systems. The cells were completely in contact with the fibers and some filopodia-like extensions of the cytoplasm were observed coming up from the cells towards the fibers (see the arrows in the Fig. 10c). Previously it has been reported that the filopodia leads the direction of the migrating cells and facilitate the intercellular communication, which suggest that the scaffold design can promote cell migration and adhesion [74,75]. Overall, the cell morphologies and the growth along the fiber scaffolds indicate a favorable cell-fiber interaction.

Regarding cell migration (Fig. 11), cells were found throughout the length of the samples and at different depth levels for the PDLLA-ZnO 5%-Hap 5% scaffold. In a sample's volume of 212 × 212 × 75 μm, the interconnected group of cells were shown at different depths, finding cells down to 37 μm depth from the surface of the material (Fig. 11-a, b). Additionally, it was clearly demonstrated how the cells interact with the fibers, located predominantly along the axial direction of the fibers (Figs. 10-b and 11-c, d). The cells localization within the fibers also showed biocompatibility, since cells were able to grow embedded within the scaffolds. Together with the viability results it can be stated that the scaffold could promote the possible exchange of nutrients and gases between the cells and the culture media at different depths within the samples due to the developed porosity, a feature that is desirable in biocompatible materials. This demonstrates a favorable design of the scaffold, fundamentally related to its chemical nature (polymer and active components), porosity and pore size distribution.

Regarding the cell proliferation and adhesion, Fig. 12 shows the results of the morphology and the number of cells obtained by the cell average found in 10 areas (212 × 212 μm). Considering that the areas with cell agglomerates were not fully deemed to determine cell proliferation, the images shown do not necessarily represent the average number of cells reported in cell proliferation (Fig. 13-d). In the positive control, which is the product of the cell interaction with a glass coverslip, the morphology of viable cells is observed with an extension of the cytoskeleton on the surface, showing evidence of cell growth (see arrow in Fig. 12, day 5) and cell division (see arrow in Fig. 12, day 7). The positive control served as a reference to confirm that the study was carried out with healthy cells, and as a basis for morphological comparison with the systems of interest. However, it must be considered that the appearance of a cell on a 2D surface will be different from that obtained on a 3D surface, and even more in the case of polymeric fibers. Due to the cells spread along the fibers and are distributed at different depth levels through the samples (Fig. 11), a different surface appearance compared to the reference is produced. The blank presented a good performance except for day 7, a behavior that favors the ternary system by presenting a sustained increase during the interaction time.

Regarding the Hap-ZnO combination, Gnaneshwar et al. [20] studied the biological effect of hybrid nHap-ZnO in electrospun polymeric fibers, in human fetal osteoblast cells (hFOB); and the authors evidenced greater biological, enzymatic and biomineralization activity in systems made up of 2% nHap-ZnO. On the other hand, Felice et al. [63] reported, through a study of the enzymatic activity of alkaline phosphatase and mineralization (generation of apatite), that ZnO could accelerate the regeneration of bone tissue. Moreover, different studies have shown that ZnO has osteoinductive and osteoconductive properties. Yusa et al. [25] reported that Zn^{2+} ions induce osteoblast differentiation through a significant increase in collagen I (the most common protein of the bone extracellular matrix), BMP-2 (bone morphogenetic protein, which induces mineralization), Runx2 (transcription factor that induces the differentiation of mesenchymal cells into osteoblasts) and VEGF-A (angiogenic factor). Our data demonstrate that fibers incorporating ZnO and/or Hap support cell adhesion and proliferation as well as fibers composed of PDLLA alone, providing a stable environment for mammalian cell growth while also providing delivery of antimicrobial agents.

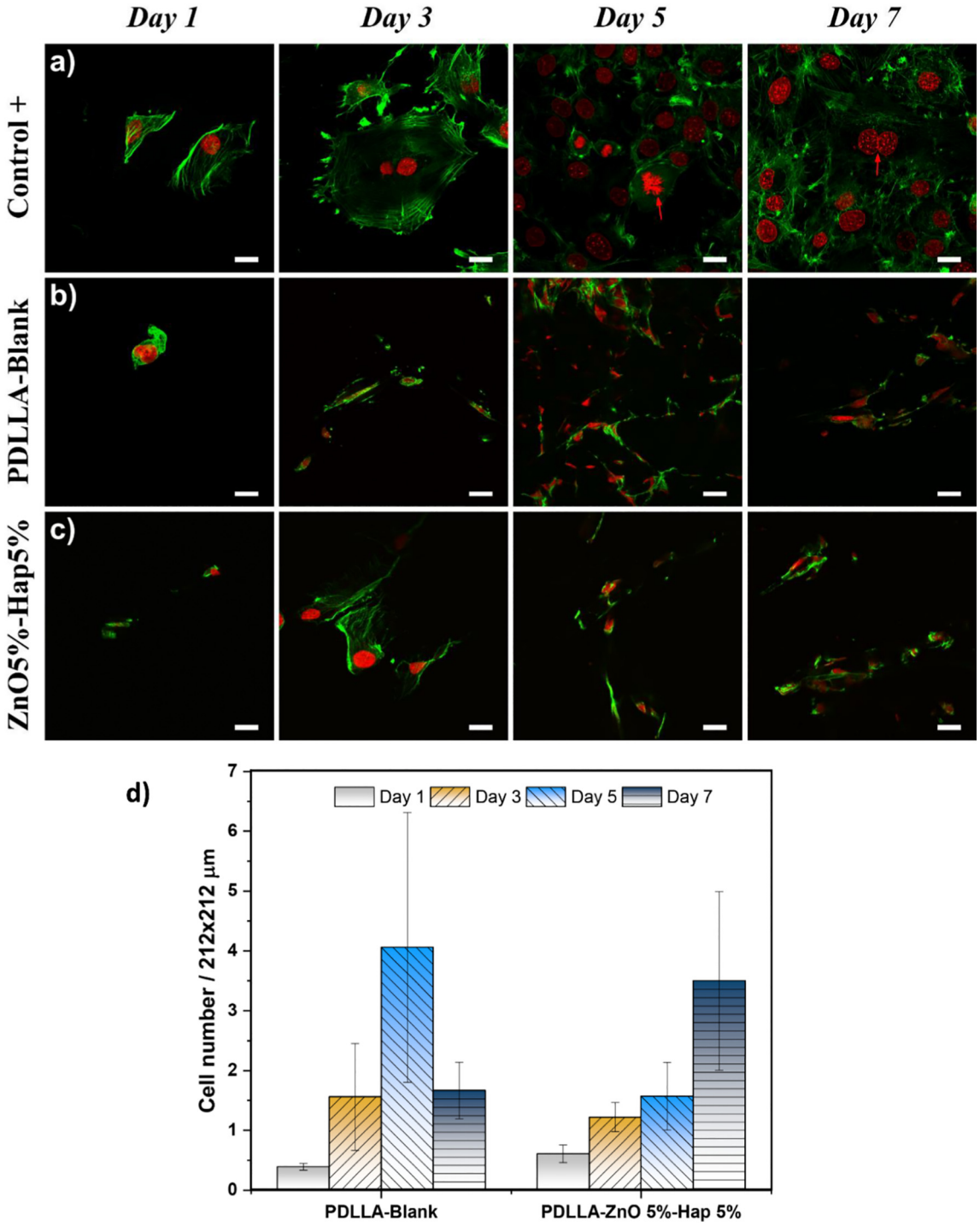

Fig. 12. Confocal micrographs showing the morphology and population growth of MC3T3-E1 cells obtained from the proliferation test at different days of scaffold-cell interaction, for control + a), PDLLA-blank (b), and PDLLA-ZnO 5%-Hap 5% fiber scaffolds (c) (scale bar: 2 μm). Proliferation of MC3T3-E1 cells (d). Cell proliferation results were obtained by the average number of cells in 10 different areas (image area: 212 × 212 μm) of the sample, selected randomly and through three replications.

4. Conclusion

PDLLA based fiber scaffolds containing ZnO and Hap nanoparticles were fabricated using the Forcespinning® technique. Rheological, morphological, thermophysical, mechanical, and biological characterization was performed on the developed fibrous composite scaffolds. The incorporation of the NPs mixture led to an increase in viscosity and a pseudo-plastic tendency of the precursor solution, which caused an increase in fiber diameter (from 0.78 ± 0.55 to 2.39 ± 0.74 μm) and its standard deviation. The rough surface characteristic of the PDLLA fibers prevailed, regardless the incorporation and concentration of NPs. S_q were of 84.1 and 109.7 nm for PDLLA blank and PDLLA-ZnO 5%-Hap 5%, respectively. The ternary systems presented a moderate dispersion of NPs, reflecting a higher level of agglomeration for ZnO. The thermal stability of PDLLA decreased due to the presence of the NPs mixture from 290 to 235 °C, in an equivalent manner to the systems formulated with only n-ZnO; that means, Hap did not interfere with the catalytic effect of ZnO on polymer degradation reactions. The antimicrobial properties of the materials were affected by the incorporation of Hap, obtaining a growth inhibition of the *E. coli* and *S. aureus* strains of 70 and 85%, respectively. Regarding cell viability, PDLLA promoted a

favorable cell response, with viabilities above 80%. In the PDLLA-ZnO 5%-Hap 5% system, the cells presented a favorable morphology and the scaffold design (porosity greater than 90% and pore size distribution from 2 to 2561.7 μm^2), promoted a sustained increase in cell proliferation in three-dimensions. The antibacterial/bioactive performance and morphological features of the obtained PDLLA-ZnO-Hap scaffold placed it as a promising candidate for applications related to bone tissue engineering.

CRediT authorship contribution statement

	Definition	Author
Conceptualization	Ideas; formulation or evolution of overarching research goals and aims	Victoria Padilla-Gainza, Graciela Morales, Heriberto Rodríguez-Tobías
Methodology	Development or design of methodology; creation of models	Victoria Padilla-Gainza, Antonio Ledezma-Pérez, Carmen Alvarado-Canché, Cristóbal Rodríguez, Robert Gilkerson.
Software	Programming, software development; designing computer programs; implementation of the computer code and supporting algorithms; testing of existing code components	Victoria Padilla-Gainza, Cristóbal Rodríguez, Raúl Loera-Valencia.
Validation	Verification, whether as a part of the activity or separate, of the overall replication/reproducibility of results/experiments and other research outputs	Victoria Padilla-Gainza, Antonio Ledezma-Pérez, Carmen Alvarado-Canché, Cristóbal Rodríguez.
Formal analysis	Application of statistical, mathematical, computational, or other formal techniques to analyze or synthesize study data	Victoria Padilla-Gainza, Cristóbal Rodríguez.
Investigation	Conducting a research and investigation process, specifically performing the experiments, or data/evidence collection	Victoria Padilla-Gainza, Cristóbal Rodríguez, Carmen Alvarado-Canché, Carlos Trevino De Leo.
Resources	Provision of study materials, reagents, materials, laboratory samples, instrumentation, computing resources, or other analysis tools	Graciela Morales, Karen Lozano, Antonio Ledezma-Pérez.
Writing - Original Draft	Preparation, creation and/or presentation of the published work, specifically writing the initial draft (including substantive translation)	Victoria Padilla-Gainza, Graciela Morales
Writing - Review & Editing	Preparation, creation and/or presentation of the published work by those from the original research group, specifically critical review, commentary or revision – including pre-or post-publication stages	Victoria Padilla-Gainza, Graciela Morales, Heriberto Rodríguez-Tobías, Raúl Loera-Valencia, Cristóbal Rodríguez, Robert Gilkerson, Karen Lozano.
Visualization	Preparation, creation and/or presentation of the published work, specifically visualization/data presentation	Victoria Padilla-Gainza, Cristóbal Rodríguez, Raúl Loera-Valencia.
Supervision	Oversight and leadership responsibility for the research activity planning and execution, including mentorship external to the core team	Graciela Morales, Heriberto Rodríguez-Tobías, Karen Lozano.
Project administration	Management and coordination responsibility for the research activity planning and execution	Victoria Padilla-Gainza, Graciela Morales
Funding acquisition	Acquisition of the financial support for the project leading to this publication	Karen Lozano, Graciela Morales

Declaration of competing interest

The authors have no conflicts of interest to disclose.

Acknowledgments

The authors acknowledge support received from National Science Foundation under PREM grant DMR 2122178 and from Consejo Nacional de Ciencia y Tecnologia (CONACYT 429352) for the scholarship granted to Victoria Padilla Gainza. The authors also thank Maria G. Mendez Padilla, Jesús G. Quiroz López and Vanessa Montaño for their technical assistance in the thermal properties, mechanical properties and guidance in the cell viability test, respectively.

Appendix A. Supplementary data

Supplementary data to this article can be found online at https://doi.org/10.1016/j.msec.2021.112594.

References

[1] M. Khakestani, S.H. Jafari, P. Zahedi, R. Bagheri, R. Hajiaghaee, Physical, morphological, and biological studies on PLA/nHA composite nanofibrous webs containing Equisetum arvense herbal extract for bone tissue engineering, J. Appl. Polym. Sci. 134 (2017) 1–10, https://doi.org/10.1002/app.45343.
[2] I. Jun, H.S. Han, J.R. Edwards, H. Jeon, Electrospun fibrous scaffolds for tissue engineering: viewpoints on architecture and fabrication, Int. J. Mol. Sci. 19 (2018), https://doi.org/10.3390/ijms19030745.
[3] D.P. Bhattarai, L.E. Aguilar, C.H. Park, C.S. Kim, A review on properties of natural and synthetic based electrospun fibrous materials for bone tissue engineering, Membranes (Basel) 8 (2018), https://doi.org/10.3390/membranes8030062.
[4] D.J. Hadjidakis, I.I. Androulakis, Bone remodeling, Ann. N. Y. Acad. Sci. 1092 (2006) 385–396, https://doi.org/10.1196/annals.1365.035.
[5] J.R. Porter, T.T. Ruckh, K.C. Popat, Bone tissue engineering: a review in bone biomimetics and drug delivery strategies, Biotechnol. Prog. 25 (2009) 1539–1560, https://doi.org/10.1002/btpr.246.
[6] S. Morelli, S. Salerno, J. Holopainen, M. Ritala, L. De Bartolo, Osteogenic and osteoclastogenic differentiation of co-cultured cells in polylactic acid-nanohydroxyapatite fiber scaffolds, J. Biotechnol. 204 (2015) 53–62, https://doi.org/10.1016/j.jbiotec.2015.03.023.
[7] U. Ripamonti, Osteoinduction in porous hydroxyapatite implanted in heterotopic site of different animal models, Biomaterials 17 (1996) 31–35, https://doi.org/10.1016/0735-1097(92)90514-N.
[8] T. Albrektsson, C. Johansson, Osteoinduction, osteoconduction and osseointegration, Eur. Spine J. 10 (2001) S96–S101, https://doi.org/10.1007/s005860100282.
[9] D.M. Ibrahim, E.S. Sani, A.M. Soliman, N. Zandi, E. Mostafavi, A.M. Youssef, N.K. Allam, N. Annabi, Bioactive and elastic nanocomposites with antimicrobial properties for bone tissue regeneration, ACS Appl. Bio Mater. 3 (2020) 3313–3325, https://doi.org/10.1021/acsabm.0c00250.
[10] G. Turnbull, J. Clarke, F. Picard, P. Riches, L. Jia, F. Han, B. Li, W. Shu, 3D bioactive composite scaffolds for bone tissue engineering, Bioact. Mater. 3 (2018) 278–314, https://doi.org/10.1016/j.bioactmat.2017.10.001.
[11] J. Ramier, T. Bouderlique, O. Stoilova, N. Manolova, I. Rashkov, V. Langlois, E. Renard, P. Albanese, D. Grande, Biocomposite scaffolds based on electrospun poly (3-hydroxybutyrate) nano fi bers and electrosprayed hydroxyapatite nanoparticles for bone tissue engineering applications, Mater. Sci. Eng. C. 38 (2014) 161–169, https://doi.org/10.1016/j.msec.2014.01.046.
[12] D. Guan, Z. Chen, C. Huang, Y. Lin, Attachment, proliferation and differentiation of BMSCs on gas-jet/electrospun nHAP/PHB fibrous scaffolds, Appl. Surf. Sci. 255 (2008) 324–327, https://doi.org/10.1016/j.apsusc.2008.06.093.
[13] K. Novotna, M. Zajdlova, T. Suchy, D. Hadraba, F. Lopot, M. Zaloudkova, T.E.L. Douglas, M. Munzarova, M. Juklickova, D. Stranska, D. Kubies, D. Schaubroeck, S. Wille, L. Balcaen, M. Jarosova, H. Kozak, A. Kromka, Z. Svindrych, V. Lisa, K. Balik, L. Bacakova, Polylactide nanofibers with hydroxyapatite as growth substrates for osteoblast-like cells, J. Biomed. Mater. Res. A 102 (2014) 3918–3930, https://doi.org/10.1002/jbm.a.35061.
[14] G. Sui, X. Yang, F. Mei, X. Hu, G. Chen, X. Deng, S. Ryu, Poly-L-lactic acid/hydroxyapatite hybrid membrane for bone tissue regeneration, Wiley Intersci. 33 (2007) 446–454, https://doi.org/10.1002/jbm.a.31166.
[15] M. Sadat-Shojai, M.T. Khorasani, A. Jamshidi, A new strategy for fabrication of bone scaffolds using electrospun nano-HAp/PHB fibers and protein hydrogels, Chem. Eng. J. 289 (2016) 38–47, https://doi.org/10.1016/j.cej.2015.12.079.
[16] M. Abrigo, P. Kingshott, S.L. McArthur, Electrospun polystyrene fiber diameter influencing bacterial attachment, proliferation, and growth, ACS Appl. Mater. Interfaces 7 (2015) 7644–7652, https://doi.org/10.1021/acsami.5b00453.
[17] O.-H. Cho, I.-G. Bae, S.M. Moon, S.Y. Park, Y.G. Kwak, B.-N. Kim, S.N. Yu, M.H. Jeon, T. Kim, E.J. Choo, E.J. Lee, T.H. Kim, S.-H. Choi, J.-W. Chung, K.-C. Kang, J.H. Lee, Y.-M. Lee, M.S. Lee, K.-H. Park, Therapeutic outcome of spinal implant infections caused by Staphylococcus aureus, Medicine (Baltimore) 97 (2018), e12629, https://doi.org/10.1097/MD.0000000000012629.

[18] M. Ribeiro, F.J. Monteiro, M.P. Ferraz, Infection of orthopedic implants with emphasis on bacterial adhesion process and techniques used in studying bacterial-material interactions, Biomatter. 2 (2012) 176–194, https://doi.org/10.4161/biom.22905.

[19] T.F. Moriarty, R. Kuehl, T. Coenye, W.-J. Metsemakers, M. Morgenstern, E.M. Schwarz, M. Riool, S.A.J. Zaat, N. Khana, S.L. Kates, R.G. Richards, Orthopaedic device-related infection: current and future interventions for improved prevention and treatment, EFORT Open Rev. 1 (2016) 89–99, https://doi.org/10.1302/2058-5241.1.000037.

[20] P.V. Gnaneshwar, S.V. Sudakaran, S. Abisegapriyan, J. Sherine, S. Ramakrishna, M.H.A. Rahim, M.M. Yusoff, R. Jose, J.R. Venugopal, Ramification of zinc oxide doped hydroxyapatite biocomposites for the mineralization of osteoblasts, Mater. Sci. Eng. C. 96 (2019) 337–346, https://doi.org/10.1016/j.msec.2018.11.033.

[21] S.E. Jin, H.E. Jin, Antimicrobial activity of zinc oxide nano/microparticles and their combinations against pathogenic microorganisms for biomedical applications: from physicochemical characteristics to pharmacological aspects, Nanomaterials 11 (2021) 1–35, https://doi.org/10.3390/nano11020263.

[22] S.M. El-Sayed, H.S. El-Sayed, O.A. Ibrahim, A.M. Youssef, Rational design of chitosan/guar gum/zinc oxide bionanocomposites based on Roselle calyx extract for ras cheese coating, Carbohydr. Polym. 239 (2020), 116234, https://doi.org/10.1016/j.carbpol.2020.116234.

[23] N.A. Al-Tayyar, A.M. Youssef, R.R. Al-Hindi, Antimicrobial packaging efficiency of ZnO-SiO2 nanocomposites infused into PVA/CS film for enhancing the shelf life of food products, Food Packag. Shelf Life 25 (2020), 100523, https://doi.org/10.1016/j.fpsl.2020.100523.

[24] Y. Xie, Y. He, P.L. Irwin, T. Jin, X. Shi, Antibacterial activity and mechanism of action of zinc oxide nanoparticles against campylobacter jejuni, Appl. Environ. Microbiol. 77 (2011) 2325–2331, https://doi.org/10.1128/AEM.02149-10.

[25] K. Yusa, O. Yamamoto, H. Takano, M. Fukuda, M. Iino, Zinc-modified titanium surface enhances osteoblast differentiation of dental pulp stem cells in vitro, Sci. Rep. 6 (2016) 1–11, https://doi.org/10.1038/srep29462.

[26] A.Rajan Unnithan, R. Arthyram, C.Sang Kim, Scaffolds with antibacterial properties, in: S. Thomas, Y. Grohens, N. Neethu (Eds.), Nanotechnol. Appl. Tissue Eng, Elsevier, United States of America 2015, pp. 103–104.

[27] G.P. Barreto, G. Morales, M.L.L. Quintanilla, Microwave assisted synthesis of ZnO nanoparticles: effect of precursor reagents, temperature, irradiation time, and additives on Nano-ZnO morphology development, J. Mater. 2013 (2013) 1–11, https://doi.org/10.1155/2013/478681.

[28] H.S. El-Sayed, S.M. El-Sayed, A.M. Youssef, Novel approach for biosynthesizing of zinc oxide nanoparticles using lactobacillus gasseri and their influence on microbiological, chemical, sensory properties of integrated yogurt, Food Chem. 365 (2021), 130513, https://doi.org/10.1016/j.foodchem.2021.130513.

[29] A. Chaudhary, N. Kumar, R. Kumar, R.K. Salar, Antimicrobial activity of zinc oxide nanoparticles synthesized from Aloe vera peel extract, SN Appl. Sci. 1 (2019) 1–9, https://doi.org/10.1007/s42452-018-0144-2.

[30] D. Virovska, D. Paneva, N. Manolova, I. Rashkov, D. Karashanova, Electrospinning/electrospraying vs. Electrospinning: a comparative study on the design of poly(l-lactide)/zinc oxide non-woven textile, Appl. Surf. Sci. 311 (2014) 842–850, https://doi.org/10.1016/j.apsusc.2014.05.192.

[31] X. Ji, T. Wang, L. Guo, J. Xiao, Z. Li, L. Zhang, Y. Deng, N. He, Effect of nanoscale-ZnO on the mechanical property and biocompatibility of electrospun poly(L-lactide) acid/nanoscale-ZnO mats, J. Biomed. Nanotechnol. 9 (2013) 417–423, https://doi.org/10.1166/jbn.2013.1556.

[32] H. Rodríguez-Tobías, G. Morales, A. Ledezma, J. Romero, D. Grande, Novel antibacterial electrospun mats based on poly(D, L-lactide) nanofibers and zinc oxide nanoparticles, J. Mater. Sci. 49 (2014) 8373–8385, https://doi.org/10.1007/s10853-014-8547-y.

[33] Y. Huang, T. Wang, X. Zhao, X. Wang, L. Zhou, Y. Yang, F. Liao, Y. Ju, Poly (lactic acid)/ graphene oxide – ZnO nanocomposite films with good mechanical, dynamic mechanical, anti-UV and antibacterial properties, J. Chem. Technol. Biotechnol. 90 (2015) 1677–1684, https://doi.org/10.1002/jctb.4476.

[34] S.Y. Hussain, H.Y. Yu, D. Wang, J. Yao, Electrospun poly(3-hydroxybutyrate-co-3-hydroxy-valerate)/cellulose reinforced nanofibrous membranes with ZnO nanocrystals for antibacterial wound dressings, Cellulose 24 (2017) 2925–2938, https://doi.org/10.1007/s10570-017-1303-0.

[35] R. Naphade, J. Jog, Electrospinning of PHBV/ZnO membranes: structure and properties, Fibers Polym. 13 (2012) 692–697, https://doi.org/10.1007/s12221-012-0692-9.

[36] W. Yu, C.H. Lan, S.J. Wang, P.F. Fang, Y.M. Sun, Influence of zinc oxide nanoparticles on the crystallization behavior of electrospun poly(3-hydroxybutyrate-co-3-hydroxyvalerate) nanofibers, Polymer (Guildf) 51 (2010) 2403–2409, https://doi.org/10.1016/j.polymer.2010.03.024.

[37] H. Rodríguez-Tobías, G. Morales, A. Ledezma, J. Romero, R. Saldívar, V. Langlois, E. Renard, D. Grande, Electrospinning and electrospraying techniques for designing novel antibacterial poly(3-hydroxybutyrate)/zinc oxide nanofibrous composites, J. Mater. Sci. 51 (2016) 8593–8609, https://doi.org/10.1007/s10853-016-0119-x.

[38] V. Stanić, S. Dimitrijević, J. Antić-Stanković, M. Mitrić, B. Jokić, I.B. Plećaš, S. Raičević, Synthesis, characterization and antimicrobial activity of copper and zinc-doped hydroxyapatite nanopowders, Appl. Surf. Sci. 256 (2010) 6083–6089, https://doi.org/10.1016/j.apsusc.2010.03.124.

[39] A.A. Shitole, P.W. Raut, N. Sharma, B. Garnaik, Electrospun polycaprolactone / hydroxyapatite / ZnO nano fi bers as potential biomaterials for bone tissue regeneration, J. Mater. Sci. Mater. Med. (2019), https://doi.org/10.1007/s10856-019-6255-5.

[40] S. Padron, A. Fuentes, D. Caruntu, K. Lozano, Experimental study of nanofiber production through forcespinning, J. Appl. Phys. 113 (2013) 24318.

[41] I. Sebe, B. Szabó, Z.K. Nagy, D. Szabó, L. Zsidai, B. Kocsis, R. Zelkó, Polymer structure and antimicrobial activity of polyvinylpyrrolidone-based iodine nanofibers prepared with high-speed rotary spinning technique, Int. J. Pharm. 458 (2013) 99–103, https://doi.org/10.1016/j.ijpharm.2013.10.011.

[42] S.K. Padron, R. Patlan, J. Gutierrez, N. Santos, T. Eubanks, Lozano, Production and characterization of hybrid BEH-PPV/PEO conjugated polymer nanofibers by ForcespinningTM, J. Appl. Polym. Sci. 125 (2012) 3610–3616.

[43] V. Padilla-Gainza, H. Rodríguez-Tobías, G. Morales, A. Ledezma-Pérez, C. Alvarado-Canché, C. Rodríguez, R. Gilkerson, K. Lozano, Processing-structure-property relationships of biopolyester/zinc oxide fibrous scaffolds engineered by centrifugal spinning, Polym. Adv. Technol. (2020) 1–14, https://doi.org/10.1002/pat.4987.

[44] V. Padilla-Gainza, G. Morales, H. Rodríguez-Tobías, K. Lozano, Forcespinning technique for the production of poly(d, l-lactic acid) submicrometer fibers: Process–morphology–properties relationship, J. Appl. Polym. Sci. 136 (2019) 1–9, https://doi.org/10.1002/app.47643.

[45] V.M. Padilla-Gainza, H. Rodríguez-Tobías, G. Morales, E. Saucedo-Salazar, K. Lozano, V. Montaño-Machado, D. Mantovani, Centrifugally spun mats based on biopolyesters/hydroxyapatite and their potential as bone scaffolds, J. Appl. Polym. Sci. 138 (2021) 1–13, https://doi.org/10.1002/app.50139.

[46] Z. Wang, C. Zhao, Z. Pan, Porous bead-on-string poly(lactic acid) fibrous membranes for air filtration, J. Colloid Interface Sci. 441 (2015) 121–129, https://doi.org/10.1016/j.jcis.2014.11.041.

[47] J.J. Rogalski, C.W.M. Bastiaansen, T. Peijs, Rotary jet spinning review–a potential high yield future for polymer nanofibers, Nanocomposites 3 (2017) 97–121, https://doi.org/10.1080/20550324.2017.1393919.

[48] S.C. Wong, A. Baji, S. Leng, Effect of fiber diameter on tensile properties of electrospun poly(ε-caprolactone), Polymer (Guildf) 49 (2008) 4713–4722, https://doi.org/10.1016/j.polymer.2008.08.022.

[49] Japanese Industrial Standard (Z 2801), Test for Antimicrobial Activity and Efficacy, 2001.

[50] H. Rokbani, A. Ajji, Rheological properties of poly (lactic acid) solutions added with metal oxide nanoparticles for electrospinning, J. Polym. Environ. 26 (2018) 2555–2565, https://doi.org/10.1007/s10924-017-1155-6.

[51] A.M. Díez-Pascual, A.L. Díez-Vicente, Poly(3-hydroxybutyrate)/ZnO bionanocomposites with improved mechanical, barrier and antibacterial properties, Int. J. Mol. Sci. 15 (2014) 10950–10973.

[52] R.E. Neuendorf, E. Saiz, A.P. Tomsia, R.O. Ritchie, Adhesion between biodegradable polymers and hydroxyapatite: relevance to synthetic bone-like materials and tissue engineering scaffolds, Acta Biomater. 4 (2008) 1288–1296, https://doi.org/10.1016/j.actbio.2008.04.006.

[53] Hydrogen bonding interaction of poly(d , l -Lactide)/hydroxyapatite nanocomposites, Chem. Mater. 19 (2007) 247–253, https://doi.org/10.1021/cm0619398.

[54] N. Othman, Rheology and Processing of Poly (Lactides) and Their Enantiomeric Copolymers and Blends, The University of British Columbia, 2012.

[55] D.W. Chae, B.C. Kim, Effects of interface affinity on the rheological properties of zinc oxide nanoparticle-suspended polymer solutions, Macromol. Res. 18 (2010) 772–776, https://doi.org/10.1007/s13233-010-0815-3.

[56] J. Oliveira, G.S. Brichi, J.M. Marconcini, L.H.C. Mattoso, G.M. Glenn, E.S. Medeiros, Effect of solvent on the physical and morphological properties of poly(lactic acid) nanofibers obtained by solution blow spinning, J. Eng. Fibers Fabr. 9 (2014) 117–125, https://doi.org/10.1177/155892501400900414.

[57] S. Migita, K. Araki, Effect of nanometer scale surface roughness of titanium for osteoblast function, AIMS Bioeng. 4 (2017) 162–170, https://doi.org/10.3934/bioeng.2017.1.162.

[58] S.G. Kumbar, R. James, S.P. Nukavarapu, C.T. Laurencin, Electrospun nanofiber scaffolds: engineering soft tissues, Biomed. Mater. 3 (2008) 1–15, https://doi.org/10.1088/1748-6041/3/3/034002.

[59] H. Rodríguez-Tobías, G. Morales, D. Grande, Improvement of mechanical properties and antibacterial activity of electrospun poly(D, L-lactide)-based mats by incorporation of ZnO-graft-poly(D, L-lactide) nanoparticles, Mater. Chem. Phys. 182 (2016) 324–331, https://doi.org/10.1016/j.matchemphys.2016.07.039.

[60] A. Anžlovar, A. Kržan, E. Žagar, Degradation of PLA/ZnO and PHBV/ZnO composites prepared by melt processing, Arab. J. Chem. (2017), https://doi.org/10.1016/j.arabjc.2017.07.001.

[61] H. Abe, N. Takahashi, K.J. Kim, M. Mochizuki, Y. Doi, Thermal degradation processes of end-capped poly(L-lactide)s in the presence and absence of residual zinc catalyst, Biomacromolecules 5 (2004) 1606–1614, https://doi.org/10.1021/bm0497872.

[62] N. Saha, K. Keskinbora, E. Suvaci, B. Basu, Sintering, microstructure, mechanical, and antimicrobial properties of HAp-ZnO biocomposites, J Biomed Mater Res B Appl Biomater 95 B (2010) 430–440, https://doi.org/10.1002/jbm.b.31734.

[63] B. Felice, M.A. Sánchez, M.C. Socci, L.D. Sappia, M.I. Gómez, M.K. Cruz, C.J. Felice, M. Martí, M.I. Pividori, G. Simonelli, A.P. Rodríguez, Controlled degradability of PCL-ZnO nanofibrous scaffolds for bone tissue engineering and their antibacterial activity, Mater. Sci. Eng. C. 93 (2018) 724–738, https://doi.org/10.1016/j.msec.2018.08.009.

[64] Y. Hong, D.G. Brown, Electrostatic behavior of the charge-regulated bacterial cell surface, Langmuir 24 (2008) 5003–5009, https://doi.org/10.1021/la703564q.

[65] N. Mitik-Dineva, J. Wang, V.K. Truong, P. Stoddart, F. Malherbe, R.J. Crawford, E.P. Ivanova, Escherichia coli, Pseudomonas aeruginosa, and Staphylococcus aureus attachment patterns on glass surfaces with nanoscale roughness, Curr. Microbiol. 58 (2009) 268–273, https://doi.org/10.1007/s00284-008-9320-8.

[66] W. Janusz, E. Skwarek, The study of the properties of the hydroxyapatite/electrolyte interface, Ann. UMCS Chem. 64 (2010), https://doi.org/10.2478/v10063-008-0003-x.

[67] J.M. Cornejo-Bravo, L.J. Villarreal-Gómez, R. Vera-Graziano, M.R. Vega-Ríos, J.L. Pineda-Camacho, H. Almaraz-Reyes, P.A. Mier-Maldonado, Biocompatibility evaluation of electrospun scaffolds of poly (L-Lactide) with pure and grafted hydroxyapatite, J. Mex. Chem. Soc. 58 (2017), https://doi.org/10.29356/jmcs.v58i4.53.

[68] J. Yu, H.-J. Kim, M.-R. Go, S.-H. Bae, S.-J. Choi, ZnO interactions with biomatrices: effect of particle size on ZnO-protein Corona, Nanomaterials 7 (2017) 377, https://doi.org/10.3390/nano7110377.

[69] F. De Giorgi, L. Lartigue, F. Ichas, Electrical coupling and plasticity of the mitochondrial network, Cell Calcium 28 (2000) 365–370, https://doi.org/10.1054/ceca.2000.0177.

[70] M. Karbowski, R.J. Youle, Dynamics of mitochondrial morphology in healthy cells and during apoptosis, Cell Death Differ. 10 (2003) 870–880, https://doi.org/10.1038/sj.cdd.4401260.
[71] D.A. Fletcher, R.D. Mullins, Cell mechanisms and cytoskeleton, Nature 463 (2010) 485–492, https://doi.org/10.1038/nature08908.Cell.
[72] A.S. Badami, M.R. Kreke, M.S. Thompson, J.S. Riffle, A.S. Goldstein, Effect of fiber diameter on spreading, proliferation, and differentiation of osteoblastic cells on electrospun poly(lactic acid) substrates, Biomaterials 27 (2006) 596–606, https://doi.org/10.1016/j.biomaterials.2005.05.084.
[73] X. Luo, S. Zhang, B. Luo, H. Li, Engineering collagen fiber templates with oriented nanoarchitecture and concerns on osteoblast behaviors, Int. J. Biol. Macromol. 185 (2021) 77–86, https://doi.org/10.1016/j.ijbiomac.2021.06.072.
[74] B. Wang, Q. Cai, S. Zhang, X. Yang, X. Deng, The effect of poly (L-lactic acid) nanofiber orientation on osteogenic responses of human osteoblast-like MG63 cells, J. Mech. Behav. Biomed. Mater. 4 (2011) 600–609, https://doi.org/10.1016/j.jmbbm.2011.01.008.
[75] R.F. Brown, D.E. Day, T.E. Day, S. Jung, M.N. Rahaman, Q. Fu, Growth and differentiation of osteoblastic cells on 13–93 bioactive glass fibers and scaffolds, Acta Biomater. 4 (2008) 387–396, https://doi.org/10.1016/j.actbio.2007.07.006.